Catalysis Today 145 (2009) 176–185

Contents lists available at ScienceDirect

Catalysis Today

journal homepage: www.elsevier.com/locate/cattod

Methane partial oxidation on NiCu-based catalysts

Loredana De Rogatis [a], Tiziano Montini [a], Andrea Cognigni [b], Luca Olivi [b], Paolo Fornasiero [a,*]

[a] Department of Chemical Sciences, Center of Excellence for Nanostructured Materials, INSTM-Trieste Research Unit, CNR-ICCOM Trieste Research Unit, University of Trieste, Via L. Giorgieri 1, 34127 Trieste, Italy
[b] Elettra, Sincrotrone Triste S.C.p.A. Strada Statale 14, Km 163.5 Basovizza, Trieste, Italy

Dedicated to Professor Julian R.H. Ross for his outstanding contribution to heterogeneous catalysis.

ARTICLE INFO

Article history:
Available online 9 June 2008

Keywords:
Methane partial oxidation
Hydrogen production
Ni- and Cu-based catalysts

ABSTRACT

Catalytic Partial Oxidation of Methane (CPOM) to synthesis gas was studied over supported NiCu-based catalysts prepared by wet impregnation procedure. The samples were characterized by means of X-ray diffraction (XRD), N_2 physisorption, CO chemisorption experiments, temperature-programmed reduction (TPR), near edge (XANES) and extended (EXAFS) X-ray absorption spectroscopy. The catalyst stability was evaluated under severe reaction conditions.

Reduced/preactivated Ni(10%)/Al_2O_3 shows complete CH_4 conversion above 700 °C, leading to a H_2/CO ratio of about 2 in the temperature range 850–900 °C. Vice versa, the catalytic activity of the calcined/oxidized sample is appreciably shifted towards higher temperature. Both calcined and reduced Cu(10%)/Al_2O_3 present very poor CPOM activity. Noteworthy, the performance of reduced Ni(5%)Cu(5%)/Al_2O_3 is significantly improved with respect to reduced Ni(10%)/Al_2O_3: the activity of bimetallic system is shifted by ~150 °C towards lower temperatures. Furthermore, temperature-programmed oxidation (TPO) experiments on CPOM-aged samples showed that carbon deposition on Ni(5%)Cu(5%)/Al_2O_3 is negligible with respect to Ni(10%)/Al_2O_3.

1. Introduction

The development of new energy strategy that could be economically and environmentally sustainable and be able to meet the demands for a broad range of services (household, commerce, industry and transportation needs) is an imperative challenge. In this context, hydrogen is considered one of the key energy carriers in terms of energy source, as fuel for transportation and intermediate in the conversion of renewable energy sources [1].

Its production represents the first step towards the transition to the hydrogen economy. In the near- and mid-term, hydrogen production from hydrocarbons seems to be the best choice to achieve a gradual transition, given that the present infrastructure can be used and a certain reduction degree of greenhouse gas emissions can be achieved.

Today hydrogen is mainly produced via Steam Reforming of Methane (SRM), a process highly endothermic and very expensive, due to the high heat demand [2]. A promising alternative reaction route, which has recently received great attention, is the Catalytic Partial Oxidation of Methane (CPOM):

$$CH_4 + \tfrac{1}{2}O_2 \rightarrow CO + 2H_2, \quad \Delta H^{\circ}_{25\,^{\circ}C} = -35.7\ \mathrm{kJ\,mol^{-1}}.$$

This process offers many advantages with respect to the conventional steam reforming: it is a weakly exothermic reaction requiring lower energy than SRM and it can operate at low contact times, allowing the use of small reactors [3].

The CPOM reaction was studied over a wide range of heterogeneous catalysts. Noble metal catalysts [4–12] and non-noble metal catalysts [13–23] have been reported to be active. Although noble metal-based systems, particularly Rh-based catalysts, show higher activity/selectivity and good long term stability, their high cost and limited availability make more practical, from industrial standpoint, the development of non-precious metal-based catalysts. Ni-based systems are very attractive in this respect. However, one major problem for these catalysts is the deactivation with time as a result of carbon deposition, nickel sintering and phase transformation.

Depending on the operation conditions and the type of catalyst employed (e.g. metal and support nature), two mechanistic schemes for CPOM were proposed. The first reaction pathway is the Direct Partial Oxidation (DPO) [24–27], in which CH_4 and O_2 decompose on the surface of the catalyst followed by recombination of adsorbed

* Corresponding author. Fax: +39 040 5583903.
E-mail address: pfornasiero@units.it (P. Fornasiero).

0920-5861/$ – see front matter © 2008 Elsevier B.V. All rights reserved.
doi:10.1016/j.cattod.2008.04.019

species to produce CO and H_2 as primary products. In this case, CO_2 and H_2O are secondary products, obtained by successive reaction of the primary products with adsorbed oxygen. The second pathway is designed as Combustion and Reforming Reactions (CRR) [15,28], which involves the total oxidation of part of the methane, followed by reforming of the remaining CH_4 with the CO_2 and H_2O produced by the combustion reaction. The water gas shift reaction is also involved. The CRR pathway is characterized by temperature gradients along the catalytic bed, since the highly exothermic combustion reaction takes place at its front, while the other reactions occur in the second part of the catalytic bed.

Ni–Cu bimetallic catalysts were intensively studied for ethanol steam reforming [29–34], methane decomposition [35–38], methane steam reforming [39], methane dry reforming [40], methanol partial oxidation [41], methanol decomposition [42], CO and CO_2 hydrogenation [43,44] and nitrogen oxides reduction [45]. It was observed that the addition of copper to nickel can significantly affect the activity, selectivity and stability of the catalysts. However, up to now, the mechanism of nickel promotion with copper is still not completely understood and the correlation between catalytic activity and composition or nanostructure of NiCu bimetallic systems has not been fully clarified. In the present study we contributed to the investigation of NiCu-based catalysts exploiting the possibility to use them for the CPOM process.

2. Experimental

2.1. Catalyst preparation

Ni/Cu metals were supported on a commercial Al_2O_3 (Sasol HP 14–150 calc. 900 °C × 24 h) by impregnation method using $Ni(NO_3)_2{\cdot}6H_2O$ (Puriss. Fluka) and $Cu(NO_3)_2{\cdot}3H_2O$ (Puriss. Fluka) as metal precursors.

Briefly, appropriate amounts of $Ni(NO_3)_2$ or/and $Cu(NO_3)_2$ were dissolved in ethanol. Aluminium oxide was added to the metal solution under continuous stirring. The obtained slurry was dried under vacuum at room temperature and the solid residue was further dried overnight at 120 °C in air. The material was calcined in a static oven at 600 °C in air for 5 h (heating/cooling rates 3 °C min^{-1}). Finally, the resulting powder was pelletized, crushed and sieved to collect the fraction smaller than 250 μm.

All the catalysts have a total nominal metal loading of 10 wt.%.

2.2. Characterization

BET surface area measurements were conducted using a Micromeritics ASAP 2020 analyser. N_2 physisorption isotherms were collected at −196 °C on 0.1 g of sample, after evacuation at 350 °C overnight.

CO chemisorption experiments were performed on a Micromeritics ASAP 2020 after cleaning pre-treatment at 500 °C for 1 h under O_2(5%) in an Ar flow followed by reduction at 750 °C in H_2(5%)/Ar for 2 h and evacuation at 400 °C for 4 h. Typically, 0.5 g of samples were used and an equilibration time of 10 min was employed. Adsorbed volumes were determined by extrapolation to zero pressure of the linear part of the adsorption isotherm (100–400 Torr) after elimination of the so-called reversible adsorption. A chemisorption stoichiometry CO:M = 1:1 and a spherical geometry were assumed.

Powder X-ray diffraction (XRD) patterns of the samples after calcination and activation/reduction at 750 °C for 2 h were recorded with a computer-controlled Philips X'Pert diffractometer using Cu Kα radiation (λ = 0.154 nm). The data were collected at 0.02° in the (2θ) range from 10° to 100°.

Temperature-programmed reduction (TPR) experiments were performed on ∼30 mg of the calcined materials. The samples were pre-treated at 500 °C for 1 h by pulsing of O_2 in an Ar flow every 75 s, then cooled to room temperature (r.t.). The O_2 pulses were stopped when the sample temperature was lower than 150 °C. H_2(5%)/Ar was admitted into the reactor and the flow allowed to stabilise for 30 min before increasing the temperature to 900 °C at 10 °C min^{-1}. H_2 uptake was monitored using a Thermal Conductivity Detector (TCD).

Near edge (XANES) and extended (EXAFS) X-ray absorption spectra were collected at the XAFS beamline at the Elettra synchrotron facility in Trieste operating at 2.0 GeV and 100–300 mA. All spectra were recorded at r.t. in transmission mode with a Si(1 1 1) double crystal monochromator and using ionization chambers as detectors. The resolving power was $E/\Delta E \times 10^4$, and the photon flux at the sample was 10^{10} photons s^{-1}. Angle/energy calibration was checked by simultaneously measuring a Ni and Cu metal foil absorption spectrum between the second and the third ionization chamber. The gas mixtures in the ionization chamber were chosen in order to optimize signal over Ni–Cu edges.

XANES spectra were recorded with an energy-sampling step from 0.1 to 1 eV and an integration time of 2 s per point over the range 8000–9500 eV for the Ni K edge and 8600–10,200 eV for the Cu K edge. The spectra at the edge jump were fitted by a linear combination of the reference materials for the d and the reduced state of Ni and Cu to estimate the molar fraction of reduced and oxidized metals [46]. EXAFS spectra were recorded with an energy-sampling step from 2 to 5 eV, and an integration time of 2 s per point over the range 8000–9500 eV for the Ni K edge and 8600–10,200 eV for the Cu K edge. Each EXAFS spectrum was acquired three times to increase statistics and for the signal-to-noise ratio optimization. XANES and EXAFS data analysis were performed with Athena and Artemis programs included in the Ifeffit packages. In order to obtain the coordination numbers and subsequently an estimation of particles size accordingly to Ref. [47], EXAFS first shell analysis was performed on calcined and reduced samples at Ni and Cu edges. A spherical shape geometry for metal particles was assumed.

2.3. Catalytic tests

Catalytic experiments were conducted at atmospheric pressure in a conventional fixed bed reactor (U-shaped quartz microreactor with internal diameter of 4 mm). Typically, 0.1 g of calcined sample were used. The temperature of the catalyst was measured with a K-type thermocouple. Gas flow rates were ∼83 mL min^{-1} to ensure GHSV values of ∼50,000 mL g^{-1} h^{-1}. The CPOM feed was composed of 2.0 vol.% CH_4 and 1.0 vol.% O_2 diluted in Ar. The products and reactants were quantified using a HPR20 Hyden mass spectrometer as detector.

Before testing the catalytic activity, the calcined materials were pre-treated under O_2(5%)/Ar at 500 °C for 1 h (40 mL min^{-1} and 10 °C min^{-1}) and activated by reduction in H_2(5%)/Ar at 750 °C for 2 h (40 mL min^{-1} and 10 °C min^{-1}). The gaseous mixture was introduced in the reactor at r.t. for 30 min, before ramping the furnace temperature to 900 °C at 5 °C min^{-1}. After 20 min at 900 °C, the furnace was cooled to r.t.

3. Results and discussion

3.1. Characterization

Table 1 summarises the main textural properties of the calcined materials. All samples present Type IV isotherms with hysteresis

Table 1
Results of N_2 physisorption at −196 °C on the samples after calcination in air at 600 °C for 5 h after metal impregnation and after aging under CPOM conditions

Sample		S_{BET}[a] ($m^2\ g^{-1}$)	d_M[b] (nm)	Cumulative pore volume ($mL\ g^{-1}$)
Al_2O_3[c]	–	97	47	0.93
Ni(10%)/Al_2O_3	Fresh	84	53	0.73
	Aged[d]	78	55	0.68
Cu(10%)/Al_2O_3	Fresh	80	56	0.77
	Aged[d]	77	57	0.75
Ni(5%)Cu(5%)/Al_2O_3	Fresh	82	55	0.71
	Aged[d]	79	55	0.70

[a] BET surface area.
[b] Pore diameter: maximum of the pore distribution.
[c] Pre-calcined at 900 °C for 24 h.
[d] Aged under CPOM condition in a run-up experiment + 65 h at 900 °C.

loops, typical of mesoporous materials [48]. The t-plot analysis indicates that the microporous volume is always negligible, while the BJH analysis reveals that the materials have a pore distribution centred approximately at 55 nm. All the supported metal catalysts have a specific surface area of ~80 $m^2\ g^{-1}$. The lower surface area and pore volume of the impregnated samples with respect to bare Al_2O_3 is consistent with the relative high metal loading (10 wt.%). Notably, the pre-calcination treatment of the Al_2O_3 support at 900 °C for 24 h leads to a significant decrease of surface area from 156 to 95 $m^2\ g^{-1}$. However, after this sintering, minor changes are observed under CPOM conditions. Certainly, the use of diluted reactants significantly minimizes possible local overheat contributing to the prevention of sintering. Nevertheless, we cannot completely role out some support sintering due to the fact that the presence of porous carbonaceous deposits could in theory compensate an eventual loss of support surface area. However, the differences are small and we prefer to avoid speculating on these aspects.

Powder XRD patterns of the samples after calcination and after activation in H_2 are presented in Fig. 1. Overlapping of the XRD peaks of the transitional aluminas complicates phase attribution, as does the low crystallinity of the support. However, the presence of γ-Al_2O_3 and θ-Al_2O_3 is evident, consistently with the medium calcination temperature [49]. Notably, α-Al_2O_3 is absent, in accordance with the relative high surface area of the samples [49].

The XRD patterns of the calcined Ni(10%)/Al_2O_3 and Cu(10%)/Al_2O_3 show the characteristic peaks of NiO (JCPDS 14-0481) and CuO (JCPDS 80-1268), respectively, in addition to those of the support. Average crystallite diameters of 7–8 nm for NiO and 25 nm for CuO were calculated applying the Scherrer's equation to the main reflections of the two oxides. Notably, partial overlapping of the aluminas peaks with those of the metal oxides can lead to partial overestimation of the crystallite size. Other phases related to Ni and Cu were not identified. In the case of the bimetallic sample, the XRD pattern indicates the formation of a solid solution with cubic structure (as for NiO). In fact, the addition of Cu leads to a shift towards higher angles of all the NiO diffraction peaks (Fig. 1).

After activation in H_2 at 750 °C, the XRD patterns of Ni(10%)/Al_2O_3 and Cu(10%)/Al_2O_3 exhibit the presence of the metallic phases with cubic structure (JCPDS 04-0850 and JCPDS 04-0836, respectively). The reflection broadening suggests an average crystallite diameter of 9–10 nm for Ni and 44 nm for Cu. In the case of Ni(5%)Cu(5%)/Al_2O_3 sample, the reduction leads to the formation of an alloy that maintains the cubic structure: in fact, the XRD pattern shows diffraction peaks in an intermediate position between that attributable to metallic Ni and Cu (see Fig. 2A). No

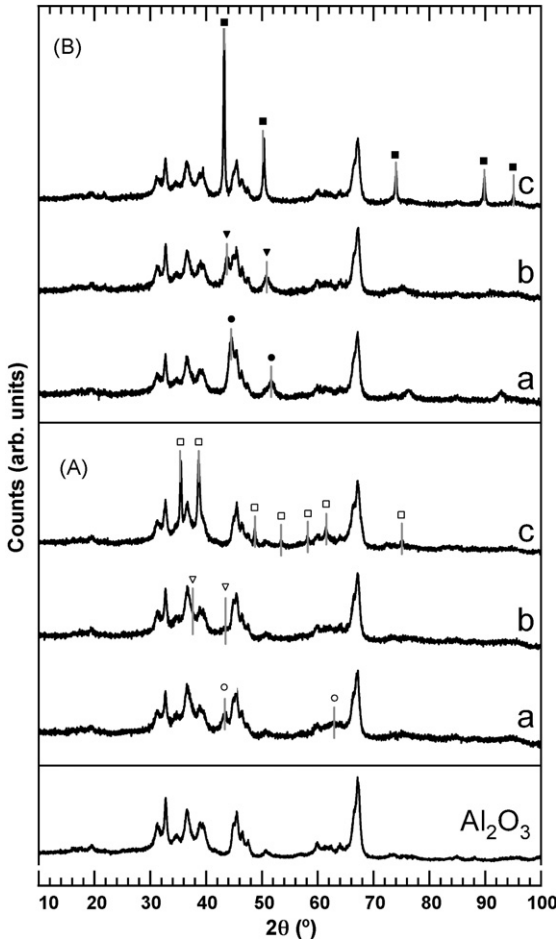

Fig. 1. XRD powder diffraction profiles of Ni(10%)/Al_2O_3 (a), Ni(5%)Cu(5%)/Al_2O_3 (b) and Cu(10%)/Al_2O_3 (c) after calcination at 600 °C for 5 h (A) and reduction at 750 °C for 2 h (B). The XRD profile of the starting Al_2O_3 is reported for comparison. (○) NiO, (▽) $NiCuO_x$, (□) CuO, (●) Ni, (▼) Ni_xCu_{1-x}, and (■) Cu.

other Ni or Cu species were detected in the XRD patterns of the reduced samples, although the presence of other phase (such as oxides or aluminates) with a high dispersion or below the detection limit cannot be excluded. Fig. 2B presents the comparison between the calculated cell parameter *a* of the metallic phases (obtained from the position of the (2 2 0) reflection) and the tabulated values for Ni and Cu and the theoretical value calculated using the Vegard's law for an alloy with composition $Ni_{0.52}Cu_{0.48}$ (calculated from the nominal loading of the two metals). For Cu, there is a good agreement between the two values, in accordance with the large crystallite size observed. Otherwise, the cell parameter of Ni and $Ni_{0.52}Cu_{0.48}$ is larger than their theoretical values. For Ni and Cu nanoparticles obtained by evaporation, a significant nearest-neighbour distance contraction was reported by Apai et al. [50]. On the other hand, Duan and Li [51] observed an expansion of the cell volume for Ni nanoparticles, as a result of the distortion of the surface atoms induced by the nanometric dimension of the particles. In this case, they attributed this result to the passivation/surface oxidation of the nanoparticles by atmospheric oxygen. A similar situation could be present also in our samples. Moreover, in the case of the reduced Cu(10%)/Al_2O_3, the presence of the passivating layer should not be observable due to larger dimensions of the crystallites.

EXAFS and XANES spectra provides useful information regarding the properties of the investigated samples. Normalised X-ray absorption coefficient of photoabsorber in a sample can be

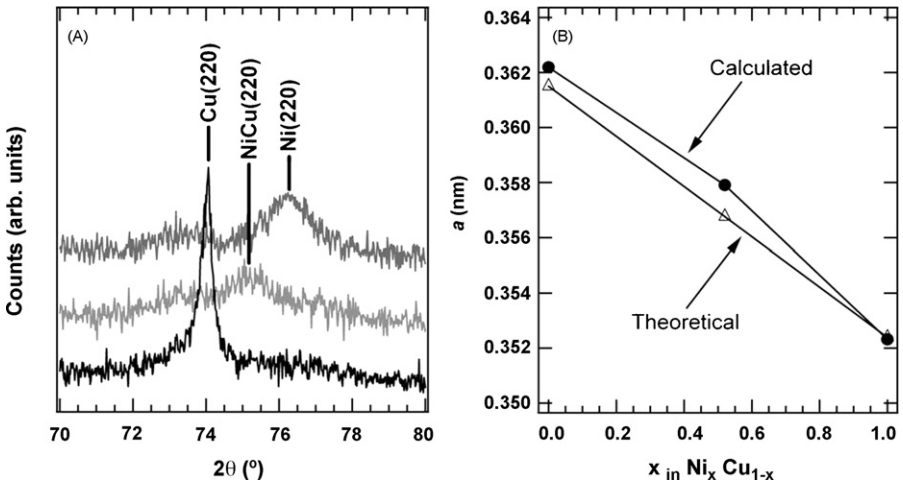

Fig. 2. (A) Detail of the range $2\theta = 70–80^\circ$ of the XRD patterns of the reduced samples, showing the shift of the (2 2 0) reflection with the composition; (B) trend of the calculated cell parameter a with the composition of the metal phase, in comparison with the theoretical value.

described as linear combination of all possible different chemical species (standard). In fact, by linear combination of the normalised XANES spectra of the standards, it was possible to reconstruct the normalised spectra of the samples and to find out weighted fraction of every component in both the calcined and reduced materials. It must be pointed out that the reduced samples were left exposed to air prior to the XAFS measurements for a few months. This leads to a significant difference between the information from the ex situ XRD, obtained immediately after the reduction treatment, and those from XAFS. Notably, the reduced samples show catalytic activity only above 400 °C. This means that the exposure of the reduced catalyst to the reaction mixture containing oxygen from r.t. significantly modify the oxidation state of the metal phase before the reaction (see below).

Fig. 3A shows XANES linear combination results of calcined Ni(10%)/Al_2O_3, with metal foil and NiO as standard, indicating that the sample is composed almost exclusively by NiO (supported on Al_2O_3). The reduced system after prolonged exposure to air (Fig. 3B) appears to be composed mainly by metal Ni(65%) and NiO(35%). This result indicates an easy surface oxidation/passivation of the Ni nanoparticles. EXAFS analysis of the calcined sample reveals a very low C.N. for the first Ni–O shell, indicating a very high dispersion of the oxide nanoparticles. This is partially in contradiction with the crystallite size obtained from XRD. This difference can be interpreted on the bases of the intrinsic characteristics/limitations of the two techniques: in fact, while EXAFS technique can average over all particles, the XRD data overestimates the contribution of the bigger and more crystalline particles with respect to the small and amorphous particles [52].

Fig. 4A reports XANES linear combination results of calcined Cu(10%)/Al_2O_3 indicating that Cu is mainly present as CuO. EXAFS first shell analysis gives a coordination number typical of bulk CuO (Table 2). The comparison of the Fourier transform of the outer shell with that of standard CuO evidences only a weak decrease in module intensity. These results are consistent with the XRD outcomes and indicates the presence of bulk CuO particles more likely with some anisotropy in the shape. After reduction, the Cu(10%)/Al_2O_3 system (Fig. 4B) contains both metal Cu(37%) and CuO(63%). The first coordination shell clearly shows the contribution of both the Cu–O shell of CuO and of the first Cu–Cu shell of metal Cu. The EXAFS fitting

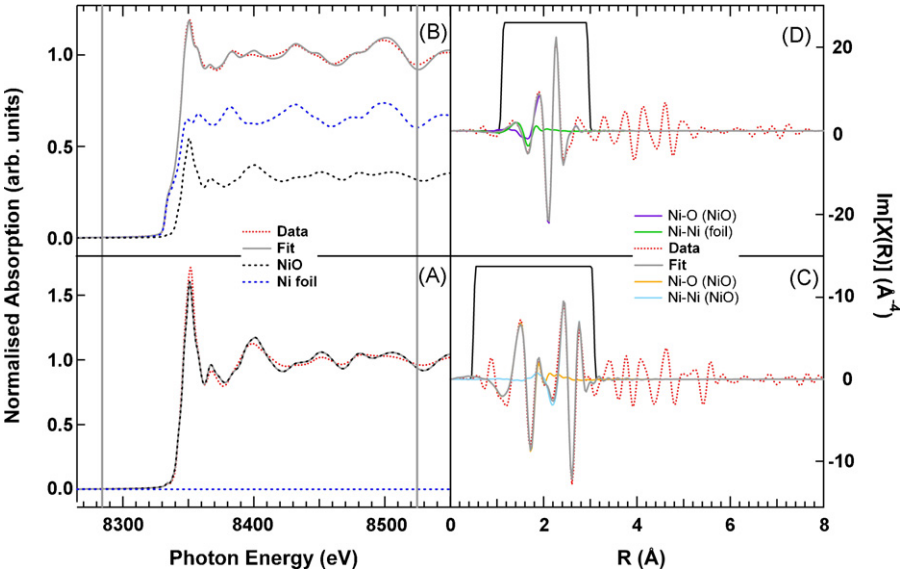

Fig. 3. Ni K-edge for Ni(10%)/Al_2O_3: experimental and fit of the XANES spectra for the calcined (A) and reduced at 750 °C for 2 h (B) samples and experimental and fit of the imaginary part of the EXFAS signal for the calcined (C) and reduced (D) samples.

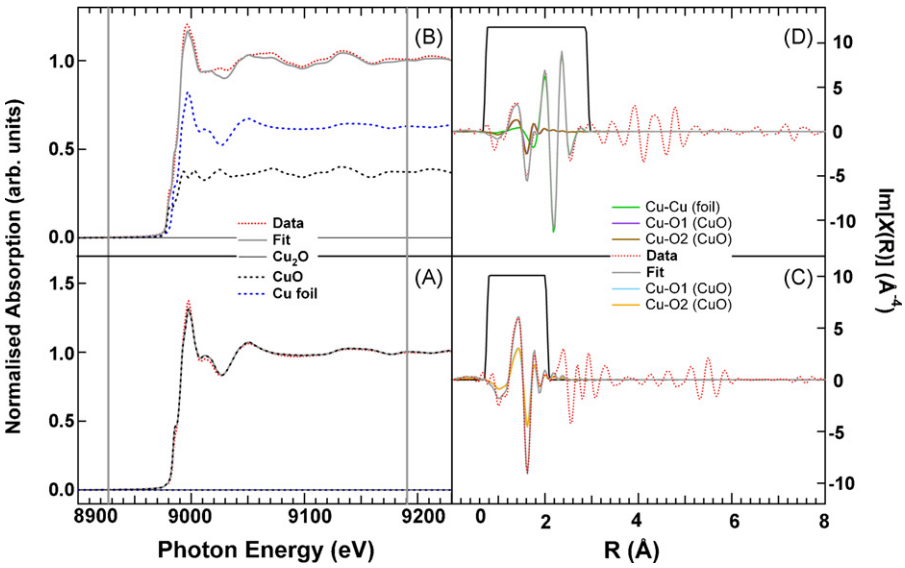

Fig. 4. Cu K-edge for Cu(10%)/Al_2O_3: experimental and fit of the XANES spectra for the calcined (A) and reduced at 750 °C for 2 h (B) samples and experimental and fit of the imaginary part of the EXFAS signal for the calcined (C) and reduced (D) samples.

Table 2
Structural parameters derived from the EXAFS analysis

Sample	Calcined			Reduced[a]		
	M–O (nm)	C.N.	M–M (nm)	C.N.	M–O (nm)	C.N.
Ni(10%)/Al_2O_3	0.208	0.5	0.248	7.1	0.203	1.8
Cu(10%)/Al_2O_3	0.195	2.0	0.254	5.2	0.195	1.0
Ni(5%)Cu(5%)/Al_2O_3[b]	0.195	1.7	0.252	3.0	0.196	2.2

[a] After treatment in flowing H_2(5%)/Ar at 750 °C for 2 h and exposure to air for a few months.
[b] Results for the analysis of the Cu edge (see text).

of this first coordination shell gives a low coordination number (Table 2), suggesting the presence of highly dispersed small Cu–CuO core–shell nanoparticles. Consistently XANES analysis indicates that the major part of Cu is oxidized.

Fig. 5 reports the results of XANES linear combination fitting at Ni and Cu edge of the calcined and reduced Ni(5%)Cu(5%)/Al_2O_3 sample. Notably, these XANES features could not be fully fitted by a linear combination of the XANES spectra of the standards. The fact that the XANES features are not completely reconstructed suggests the presence of at least another phase, which cannot be fitted by means of a combination of the pure standards. Consistently, XRD analysis points out the formation of a solid solution between NiO and CuO in the calcined system and of an alloy in the reduced one. In the calcined sample (Fig. 5A and C), the experimental data were fitted using a combination of the XANES spectra of NiO and CuO. The present data do not disagree with the formation of a solid solution between the two oxides. However, the fitting limitations (see above) do not allow further indications. In the case of reduced system (Fig. 5B and D), the best linear fitting at both edges shows a mixed composition dominated by the oxidized metals (~70% in

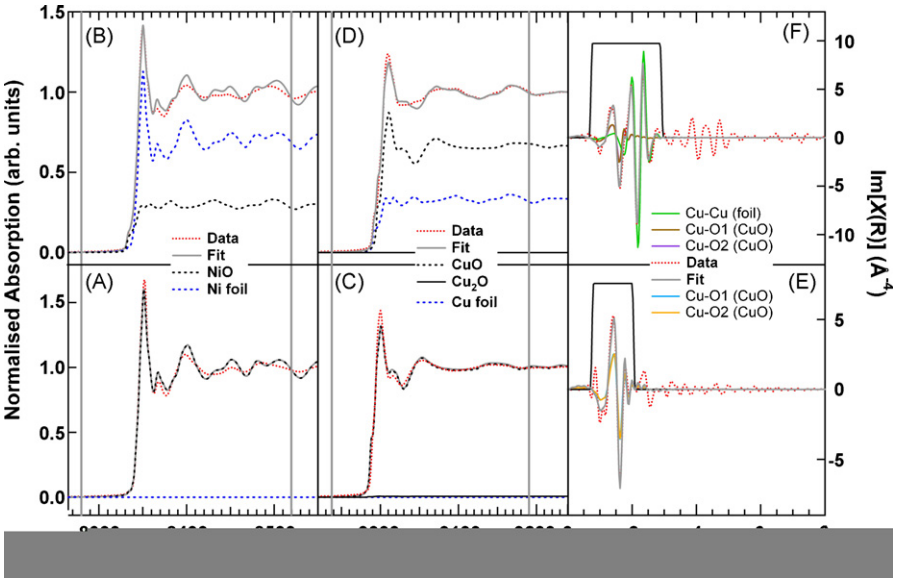

Fig. 5. Ni/Cu K-edges for Ni(5%)Cu(5%)/Al_2O_3: experimental and fit of the XANES spectra of the Ni XANES for the calcined (A) and reduced at 750 °C for 2 h (B) samples, experimental and fit of the XANES spectra of the Cu XANES for the calcined (C) and reduced (D) samples and experimental and fit of the imaginary part of the Cu EXFAS signal for the calcined (E) and reduced (F) samples.

Table 3
Metal dispersion, metallic surface area and particle size obtained from CO chemisorption

Sample	Metal dispersion (%)	Metal surface area ($m^2\ g^{-1}$)	Particle size (nm)[a]
$Ni(10\%)/Al_2O_3$	4.4	2.87	23
$Cu(10\%)/Al_2O_3$	2.4	1.55	43
$Ni(5\%)Cu(5\%)/Al_2O_3$	4.1	2.67	25

[a] Assuming a spherical geometry and CO:M = 1:1 stoichiometry.

both cases). This fact suggests that the surface oxidation/passivation is not selective and presumably a mixed oxide is formed as a shell around a residual core of the NiCu alloy. Notably, only the Cu EXAFS signal of the bimetallic system can be analysed because of the adjacent position of Ni and Cu edges, which limits the extension of the Ni edge to only 600 eV. A low coordination number for Cu–Cu is obtained in the reduced sample further suggesting the formation of a small metallic core, in agreement with the high amount of oxide species revealed by XANES.

In order to further investigate the accessibility of the metal nanoparticles, CO chemisorption experiments were performed. The data reported in Table 3 indicates that Ni and NiCu systems present comparable exposed metal surface area, while the Cu system has a very low metal dispersion. The average metal particle, estimated by assuming a spherical geometry and a CO:M ratio of 1:1, is significantly higher with respect to the crystallite size obtained from the XRD. This can be interpreted considering that the particles are composed by more crystallites and by the fact that part of the particles are in contact with the support. The trend confirms that the Cu particles are significantly bigger than those of the other two samples.

The TPR spectra of the investigated samples are shown in Fig. 6. Even though the position of the reduction peak strongly depends on many important parameters, such as the particle dimensions or the interaction strength between metal particles and the support, the TPR patterns of pure NiO, CuO, Cu_2O and NiO/CuO physical mixture are also reported for qualitative comparison.

Calcined $Ni(10\%)/Al_2O_3$ displays a broad multipeak reduction profile in the temperature range 400–800 °C. This suggests the presence of a mixture of NiO_x species originated by the different interaction of NiO particles with the Al_2O_3 support. Furthermore, the different reduction temperature could be partially ascribed to a different dimension of NiO particles. Generally, on Ni-based catalysts the low temperature H_2 uptakes are attributed to the reduction of the NiO particles weakly interacting with the support, while the high temperature ones are assigned to the reduction of NiO species in intimate contact with the support and/or forming new species such as $NiAl_2O_4$ [53–55]. Calcined $Cu(10\%)/Al_2O_3$ shows two reduction peaks at 130 and 180 °C. These two components are shifted towards lower temperature with respect to pure bulk CuO, which exhibits two reduction peaks at significantly higher temperature (in our case at 240 and 315 °C). Also pure bulk Cu_2O presents a single reduction peak at higher temperatures, in our case at 350 °C. Consistently with the XRD data, the TPR profile of the calcined $Cu(10\%)/Al_2O_3$ suggests the absence of Cu_2O. Even though the selection of adequate baseline is not straightforward, H_2 uptake supports the presence of CuO. The comparison of the TPR profile of $Ni(5\%)Cu(5\%)/Al_2O_3$ with that of $Ni(10\%)/Al_2O_3$ clearly indicates that the addition of Cu strongly promotes Ni reduction. In fact, even a physical mixture of bulk NiO and CuO shows a significant promotion of the NiO reduction. Consistently, the supported bimetallic system presents a sharp reduction peak at about 160 °C, which can be associated with the reduction of Cu in well-dispersed mixed oxide species. Furthermore a broad peak at intermediate temperature (about 350 °C) is observed. This latter process can be associated with the reduction of Ni-based species promoted by the presence of metallic Cu [40]. Finally, a minority reduction contribution is observed at high temperature, which could be either related to the presence of traces of Ni oxides species strongly interacting with the Al_2O_3 or to some kind of buoyancy effect.

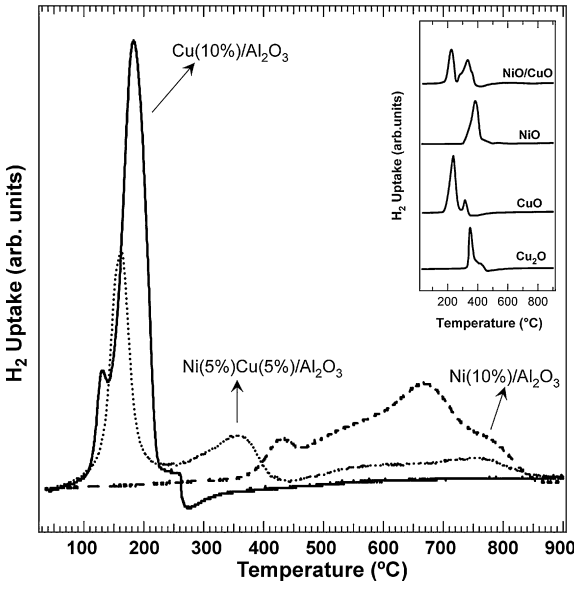

Fig. 6. TPR profiles of calcined $Ni(10\%)/Al_2O_3$, $Cu(10\%)/Al_2O_3$ and $Ni(5\%)Cu(5\%)/Al_2O_3$ after standard cleaning procedure. In the inset, the TPR profile for the reference materials are reported for comparison.

3.2. Catalytic activity

The contribution of Al_2O_3 to CPOM is marginal under our experimental conditions. In fact, on bare Al_2O_3 (data not reported) the conversion of CH_4 and O_2 starts only above 650 °C leading to maximum CH_4 and O_2 conversions of about 30% and 85%, respectively (at 900 °C).

Fig. 7 reports the activity profile of calcined (A) and reduced (B) $Ni(10\%)/Al_2O_3$ under CPOM conditions. In the case of $Ni(10\%)/Al_2O_3$ after activation in H_2 at 750 °C, O_2 is consumed between 200 and 300 °C while this does not occur for CH_4. No products are detected in this temperature range indicating the oxidation of reduced Ni particles to NiO_x species as previously reported [56]. At about 340 °C, CH_4 and O_2 start to be simultaneously converted. Up to 620 °C, temperature at which O_2 conversion reaches 100% and CH_4 conversion is approximately 25%, CO_2 and H_2O are the only observed products. This is consistent with the occurrence of total combustion of CH_4. At the "critical temperature" of 710 °C, a transient process takes place: a steep increase in CH_4 conversion is detected. This is accompanied by the formation of additional CO_2 and H_2O, and simultaneously, H_2 and CO sharply increases. Above 710 °C, H_2 and CO yields rapid increase until they reach their maximum theoretical value, while CO_2 and H_2O yields decrease to zero. The transient phenomenon described above is also detected in the case of calcined $Ni(10\%)/Al_2O_3$. However, consistently with the fact that the Ni is already oxidized, the low temperature O_2 consumption is not observed and the reactivity is shifted to higher temperatures (~100 °C). The conversions of both CH_4 and O_2 start only above 450 °C, increasing with the rise of temperature up to 775 °C when they become complete. No modification of the catalytic activity was observed during the second run-up experiment up to 900 °C on both the systems.

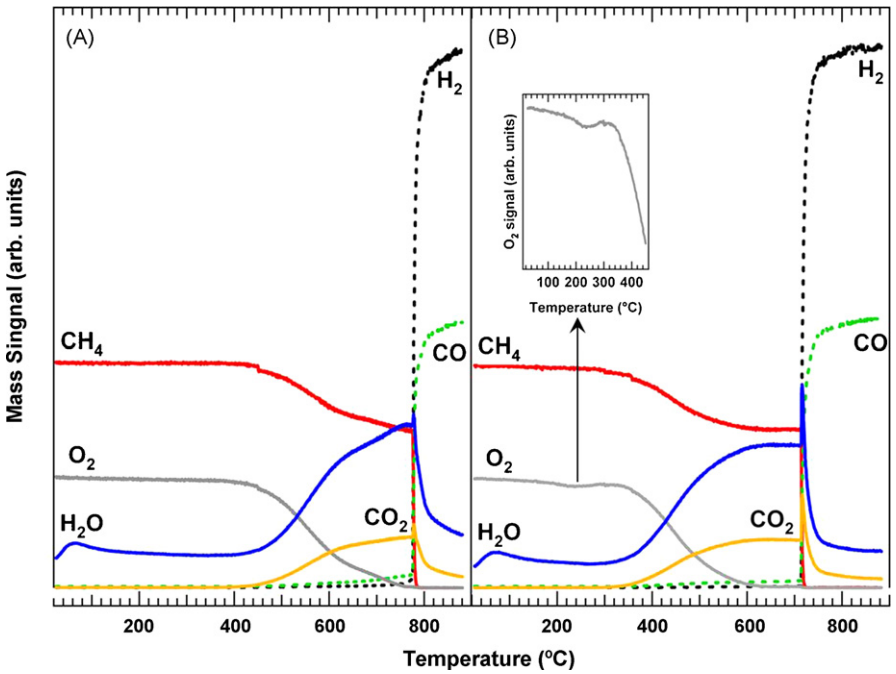

Fig. 7. Catalytic Partial Oxidation of Methane over reduced (A) and calcined (B) $Ni(10\%)/Al_2O_3$. *Conditions*: $CH_4(2.0\%) + O_2(1.0\%)$ in Ar and GHSV = 50,000 mL g^{-1} h^{-1}.

Calcined and reduced $Cu(10\%)/Al_2O_3$ show very poor CPOM activity as depicted in Fig. 8. The CH_4 and O_2 conversions begin around 350 °C, being CO_2 and H_2O the only detected products up to 700 °C. Above this temperature, H_2 and CO formation is also observed. Notably, the complete conversion of CH_4 is never achieved (~60% at 900 °C), while O_2 conversion reaches 100% at 600 °C. During the second run-up experiment, H_2 and CO yields decrease significantly suggesting catalyst deactivation. The observed deactivation could be reasonable related to metal sintering since Cu has a low coking tendency [40,57].

The catalytic performance of $Ni(5\%)Cu(5\%)/Al_2O_3$ catalyst (Fig. 9) is very promising. On the reduced sample, O_2 consumption is observed at considerably lower temperature (~45 °C) with respect to the Ni-only system. This consumption continues up to about 270 °C and it can be related to the partial oxidation of NiCu alloy particles. The concomitant conversions of CH_4 and O_2 start above 320 °C. Up to 540 °C, only CO_2 and H_2O are detected. At this temperature, complete conversion is achieved for O_2 and, simultaneously, H_2 and CO sharply increases. It is interesting to note that, in the case of $Ni(10\%)/Al_2O_3$, the O_2 conversion reaches

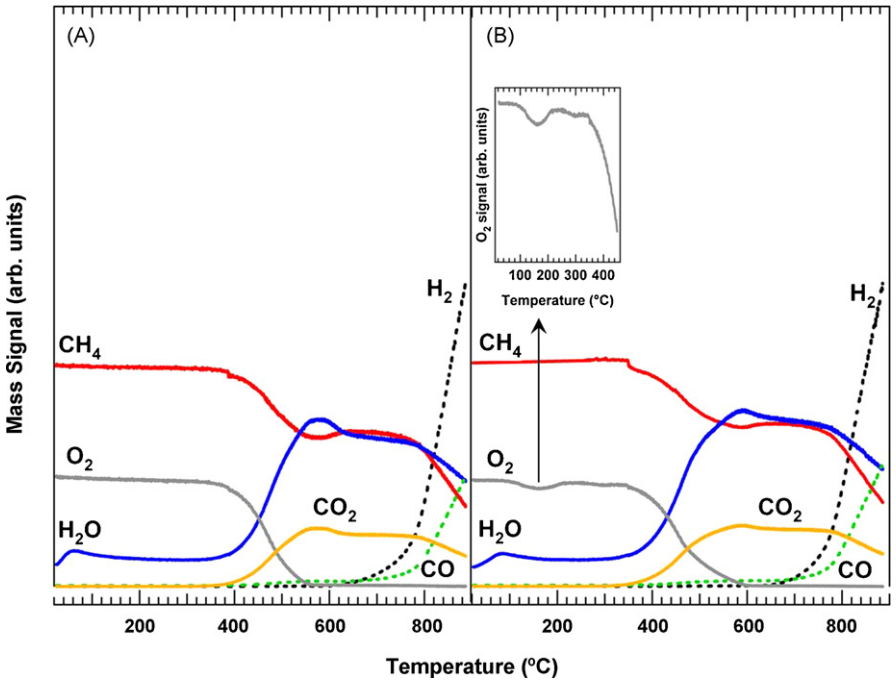

Fig. 8. Catalytic Partial Oxidation of Methane over reduced reduction at 750 °C for 2 h (A) and calcined (B) $Cu(10\%)/Al_2O_3$. *Conditions*: $CH_4(2.0\%) + O_2(1.0\%)$ in Ar and GHSV = 50,000 mL g^{-1} h^{-1}.

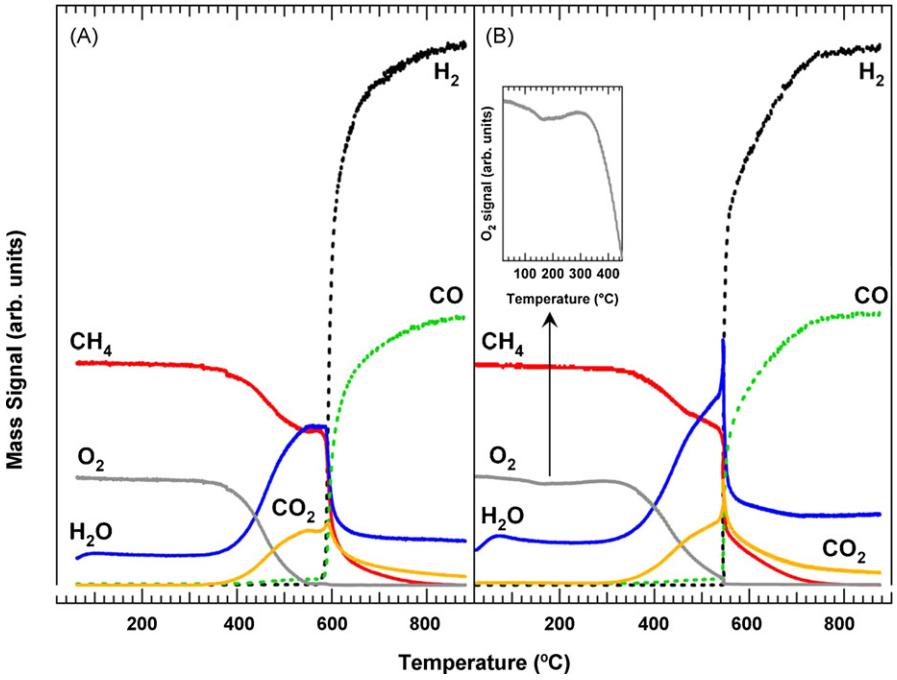

Fig. 9. Catalytic Partial Oxidation of Methane over reduced at 750 °C for 2 h (A) and calcined (B) Ni(5%)Cu(5%)/Al_2O_3. *Conditions*: CH_4(2.0%) + O_2(1.0%) in Ar and GHSV = 50,000 mL g^{-1} h^{-1}.

100% before the "critical temperature" but this does not occur for bimetallic system. At 540 °C, CH_4 conversion rapidly increases reaching 75% and becomes complete only above 750 °C. Over non-reduced Ni(5%)Cu(5%)/Al_2O_3, the sharp syngas production kick-off is shifted towards higher temperature of about 50 °C (~590 °C).

Stability tests on Ni(10%)/Al_2O_3 and Ni(5%)Cu(5%)/Al_2O_3 were conducted under reaction conditions at 900 °C for 65 h. The Cu(10%)/Al_2O_3 was not investigated due to its poor activity. No appreciable deactivation was observed for both systems, mainly because of the diluted reaction conditions. However, performing a temperature-programmed oxidation (TPO) of the aged samples, CO_2 evolution was observed only for Ni(10%)/Al_2O_3 indicating the presence of carbonaceous deposits on the catalyst surface (Fig. 10). This is consistent with the well-known ability of Ni to promote coke formation, even in the form of long filaments [58].

Partial oxidation of methane over Ni/Al_2O_3 was extensively studied in literature [15,17,19,21,56,59–64]. Using the pulse method, temperature-programmed surface reaction (TPSR) and XRD techniques on Ni(8 wt.%)/α-Al_2O_3, it was proposed by Jin et al. that the reaction follows a mechanism in which Ni^0 is first oxidized to NiO [56]. Over NiO, the complete combustion of CH_4 takes place. At a certain critical temperature, besides the complete oxidation of methane, the reduction of NiO into Ni^0 by CH_4 occurs, leading to the formation of additional CO_2 and H_2O. This nickel valence change represents the driving force, which transforms the reaction from the complete oxidation to the partial oxidation of methane. Ni^0 species constitute the active sites for the CPOM.

Our experimental data for Ni(10%)/Al_2O_3 catalyst are in agreement with this scenario. XRD and XANES revealed that the calcined Ni(10%)/Al_2O_3 contains essentially NiO well dispersed on the surface. On the other hand, the reduced sample contains Ni^0 nanoparticles, which react with O_2 during CPOM experiments up to 350 °C, producing a system similar to that observed by XANES (reduced sample exposed to air for a few months). The complete combustion of CH_4 takes place on NiO as previously reported [56,60], while the reforming of CH_4 is promoted by Ni reduced *in situ* at high temperature. In the case of the reduced Ni(10%)/Al_2O_3, the catalyst is active at lower temperature because of the presence of residual reduced Ni, which could activate CH_4 for the combustion.

In order to corroborate the reaction mechanism described above, we performed additional experiments on the reduced Ni(10%)/Al_2O_3 sample (Fig. 11A and B). After the run-up experiment (solid line in Fig. 11A analogous to Fig. 7B), the catalyst was cooled down to 380 °C under the reactant mixture (dotted line in

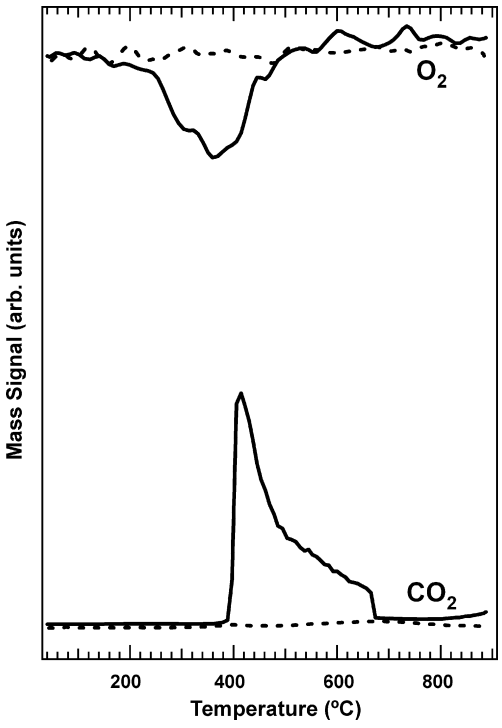

Fig. 10. Temperature-programmed oxidation (TPO) experiments on samples aged under CPOM conditions (as reported for run-up experiments) at 900 °C for 65 h: (bold line) Ni(10%)/Al_2O_3 and (dotted line) Ni(5%)Cu(5%)/Al_2O_3.

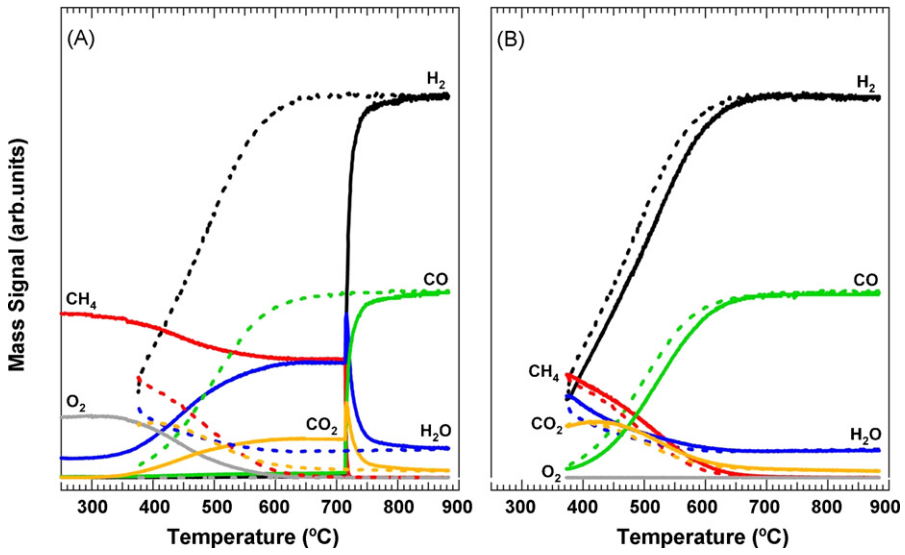

Fig. 11. Catalytic Partial Oxidation of Methane over reduced (750 °C for 2 h) Ni(10%)/Al_2O_3: (A) (solid line) run-up experiment followed by (dotted line) cooling at 380 °C under reactant mixture; (B) (bold line) subsequent run-up experiment. *Conditions*: CH_4(2.0%) + O_2(1.0%) in Ar, and GHSV = 50,000 mL g^{-1} h^{-1}.

Fig. 11A and B). Then, a second run-up experiment was carried out (solid line in Fig. 11B). The data clearly indicate that the reactivity is strongly different. Indeed, during the second run-up experiment, the 710 °C "critical temperature", which characterizes the first run-up experiment, is not observed. It is reasonable to attribute this behaviour to the absence of NiO species on the catalyst surface after high temperature treatment (reducing conditions). The trend of the H_2O and CO_2 signals could suggest a CRR mechanism. In the 380–450 °C temperature range, water is consumed via the steam reforming reaction, while the CO_2 signal remains almost constant. Only above 450 °C, the CO_2 signal starts to decrease due to the dry reforming process, which becomes operative. Furthermore, if the reduced Ni(10%)/Al_2O_3 sample is heated under inert atmosphere up to 655 (55 °C below the "critical temperature") and exposed to the reactant mixture, complete conversion of CH_4 and O_2 is instantaneously achieved as shown in Fig. 12. This fact further supports the idea that Ni^0 species on the catalyst surface promote CPOM.

Several parameters have to be taken into account to fully discuss the origin of the catalytic performance observed over the bimetallic system. Generally, the different catalytic behaviour of NiCu-based systems has been discussed in terms of two mechanisms: an electronic effect and a geometric effect [65–69]. The former is related to the differences of electronic properties of Ni–Cu alloy in comparison with individual metals. Instead, the latter effect is related to the fact that reactions such as CH_4 activation are structure-sensitive and there is a dependence on the catalyst particle size. Particles with different shapes or sizes expose different surface planes to the reactant and each of them can show a peculiar catalytic activity due to different active sites involved. These aspects require further investigation.

The run-up experiments on NiCu-based catalyst suggest that the reaction pathway is similar to that observed for Ni(10%)/Al_2O_3 implying, also in this case, a change in the oxidation state of the metals. Noteworthy, the maximum H_2/CO ratio of about 2 is achieved at ~750 °C, while on Ni(10%)/Al_2O_3 temperatures higher than 850 °C are required. The major advantage of Cu addition into the formulation of the catalyst is the strongly reduced deposition of coke. It was previously reported that coke deposition is strongly influenced by the particle size of Ni, being strongly favoured on particles larger than 7 nm [70]. This fact indicates that coke deposition requires a sufficient number of adjacent sites for carbon growth. Moreover, Chin et al. [71] reported that the addition of Au to Ni-based catalyst for hydrocarbon steam reforming prevents the catalyst deactivation, presumably by adsorption of Au on steps and edges of the Ni surfaces, sites that also represent the nucleation sites for coke deposition. Similar could be the situation in our NiCu-based system, suggesting that the effect of Cu could be mainly geometric. In fact, the formation of a Ni–Cu alloy could be responsible for the blocking or decrease of the sites involved in the carbon growth, as previously discussed by Reshetenko et al. for high temperature methane decomposition [38]. Therefore, Cu in

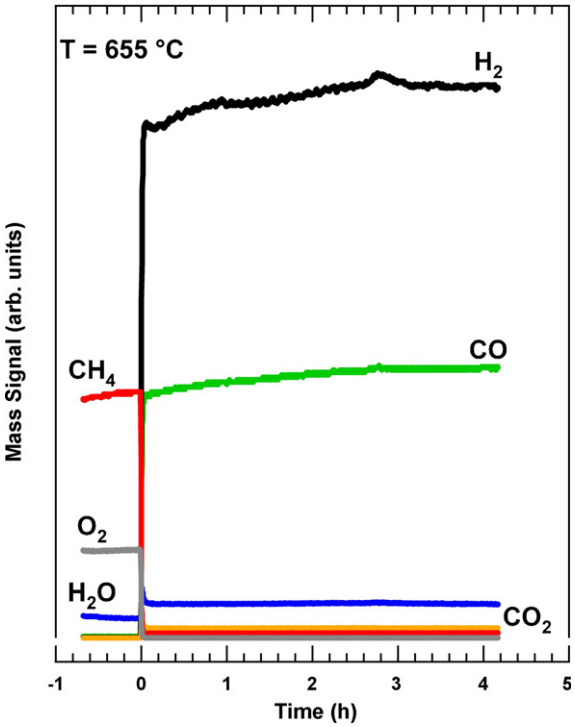

Fig. 12. Catalytic Partial Oxidation of Methane over reduced (750 °C for 2 h) Ni(10%)/Al_2O_3. Sample heated up to 655 °C under Ar. At t = 0 the sample is exposed to reactant mixture. *Conditions*: CH_4(2.0%) + O_2(1.0%) in Ar, GHSV = 50,000 mL g^{-1} h^{-1}, and T = 655 °C.

the Ni/Al_2O_3 system should act as a stabilizing agent due its structure-forming properties.

4. Conclusions

The present study highlights the promising performance of supported $NiCu/Al_2O_3$ systems for hydrogen production through CPOM. In particular the main findings can be summarized as follows:

- The impregnation of alumina with Ni or/and Cu nitrates, followed by calcinations, leads to the formation of metal oxides. XRD, CO chemisorption and XAFS data indicate higher metal dispersion in the case of Ni and NiCu systems, while relatively lower dispersion is observed for the $Cu(10\%)/Al_2O_3$ system.
- The interaction with the support and the concomitant presence of the two metals strongly promotes the reducibility of the material.
- Easy passivation/reoxidation of the reduced supported metals was observed.
- The activity results for $Ni(10\%)/Al_2O_3$ and $Ni(5\%)Cu(5\%)/Al_2O_3$ are consistent with a reaction scheme which involves first the oxidation of metallic species at low temperature ($<300\,^{\circ}C$) followed by a second step in which the metal oxide particles are reduced at a "critical temperature". Total combustion of CH_4 occurs on the oxidized particles, while partial oxidation, with H_2 and CO production in a ratio 2 to 1, is operative on reduced particles.
- A significant lowering of the light-off temperature (temperature corresponding to 50% conversion) is observed for the bimetallic system. This improvement is associated with the formation of an alloy between Ni and Cu. The formation of the alloy strongly reduces the coke deposition under CPOM conditions, increasing the life-time of the catalyst.

Acknowledgements

Prof. M. Graziani is acknowledged for the helpful discussion. University of Trieste, INSTM, FISR2002 "Nanosistemi inorganici ed ibridi per lo sviluppo e l'innovazione di celle a combustibile" are acknowledged for the financial support.

References

[1] R.M. Navarro, M.A. Pena, J.L.G. Fierro, Chem. Rev. 107 (2007) 3952.
[2] M.E.S. Hegarty, A.M. O'Connor, J.R.H. Ross, Catal. Today 42 (1998) 225.
[3] P. Ferreira-Aparicio, M.J. Benito, J.L. Sanz, Catal. Rev. Sci. Eng. 47 (2005) 491.
[4] P. Pantu, K. Kim, G.R. Gavalas, Appl. Catal. A 193 (2000) 203.
[5] O.V. Buyevskaya, K. Walter, D. Wolf, M. Baerns, Catal. Lett. 38 (1996) 81.
[6] D.Z. Wang, Z.L. Li, C.R. Luo, W.Z. Weng, H.L. Wan, Chem. Eng. Sci. 58 (2003) 887.
[7] F. Basile, G. Fornasari, M. Gazzano, A. Kiennemann, A. Vaccari, J. Catal. 217 (2003) 245.
[8] S. Albertazzi, P. Arpentinier, F. Basile, P. Del Gallo, G. Fornasari, D. Gary, A. Vaccari, Appl. Catal. A 247 (2003) 1.
[9] F. Basile, G. Fornasari, V. Rosetti, E. Trifiro, A. Vaccari, Catal. Today 91–92 (2004) 293.
[10] Y. Boucouvalas, Z.L. Zhang, X.E. Verykios, Catal. Lett. 40 (1996) 189.
[11] J.D. Grunwaldt, A. Baiker, Catal. Lett. 99 (2005) 5.
[12] T. Montini, A.M. Condò, N. Hickey, F.C. Lovey, L. De Rogatis, P. Fornasiero, M. Graziani, Appl. Catal. B 73 (2007) 84.
[13] W.L. Chu, W.S. Yang, L.W. Lin, Appl. Catal. A 235 (2002) 39.
[14] S.L. Liu, G.X. Xiong, S.S. Sheng, W.S. Yang, Appl. Catal. A 198 (2000) 261.
[15] D. Dissanayake, M.P. Rosynek, K.C.C. Kharas, J.H. Lunsford, J. Catal. 132 (1991) 117.
[16] P. Leroi, E. Madani, C. Pham-Huu, M.J. Ledoux, S. Savin-Poncet, J.L. Bousquet, Catal. Today 91-92 (2004) 53.
[17] P. Kim, Y. Kim, H. Kim, I.K. Song, J. Yi, Appl. Catal. A 272 (2004) 157.
[18] T. Shishido, M. Sukenobu, H. Morioka, M. Kondo, Y. Wang, K. Takaki, K. Takehira, Appl. Catal. A 223 (2002) 35.
[19] S. Xu, R. Zhao, X.L. Wang, Fuel Process. Technol. 86 (2004) 123.
[20] S. Xu, X.L. Wang, Fuel 84 (2005) 563.
[21] D. Ma, D.J. Mei, X. Li, M.C. Gong, Y.Q. Chen, J. Rare Earth 24 (2006) 451.
[22] V.R. Choudhary, B.S. Uphade, A.S. Mamman, Catal. Lett. 32 (1995) 387.
[23] H.Y. Wang, E. Ruckenstein, J. Catal. 199 (2001) 309.
[24] D.A. Hickman, L.D. Schmidt, J. Catal. 138 (1992) 267.
[25] D.A. Hickman, L.D. Schmidt, Science 259 (1993) 343.
[26] M. Huff, P.M. Torniainen, L.D. Schmidt, Catal. Today 21 (1994) 113.
[27] D.A. Hickman, E.A. Haupfear, L.D. Schmidt, Catal. Lett. 17 (1993) 223.
[28] M. Prettre, C. Eichner, M. Perrin, Trans. Faraday Soc. 46 (1946) 335.
[29] A. Carrero, J.A. Calles, A.J. Vizcaino, Appl. Catal. A 327 (2007) 82.
[30] A.J. No, A. Carrero, J.A. Calles, Int. J. Hydrogen Energy 32 (2007) 1450.
[31] T.A. Maia, J.D.A. Bellido, E.M. Assaf, J.M. Assaf, Quim. Nova 30 (2007) 339.
[32] F. Marino, G. Baronetti, M. Jobbagy, M. Laborde, Appl. Catal. A 238 (2002) 41.
[33] F. Marino, M. Boveri, G. Baronetti, M. Laborde, Int. J. Hydrogen Energy 26 (2001) 665.
[34] F. Marino, M. Jobbagy, G. Baronetti, M. Laborde, Stud. Surf. Sci. Catal. 130 C (2000) 2147.
[35] Y. Echegoyen, I. Suelves, M.J. Zaro, R. Moliner, J.M. Palacios, J. Power Sources 169 (2007) 150.
[36] J. Chen, Y. Li, Z. Li, X. Zhang, Appl. Catal. A 269 (2004) 179.
[37] J. Li, G. Lu, K. Li, Chem. Lett. 33 (2004) 652.
[38] T.V. Reshetenko, L.B. Avdeeva, Z.R. Ismagilov, A.L. Chuvilin, V.A. Ushakov, Appl. Catal. A 247 (2003) 51.
[39] T.J. Huang, S.Y. Jhao, Appl. Catal. A 302 (2006) 325.
[40] J.H. Lee, E.G. Lee, O.S. Joo, K.D. Jung, Appl. Catal. A 269 (2004) 1.
[41] J.Y. Xi, G.-X. Lu, Z.F. Wang, Acta Phys. Chim. Sin. 17 (2001) 658.
[42] J.Y. Xi, Z.F. Wang, W.P. Wang, G.-X. Lu, Acta Phys. Chim. Sin. 18 (2002) 82.
[43] S.H. Zhong, X.T. Wang, L.X. Mi, X.F. Xiao, J. Fuel Chem. Technol. 29 (2001) 154.
[44] Y. Wang, S. Qi, Y. Hou, React. Kinet. Catal. Lett. 70 (2000) 213.
[45] V.N. Efremov, T.A. Zinoveva, G.M. Tesakova, V.I. Yagodkin, E.Z. Golosman, Russ. J. Appl. Chem. 73 (2000) 257.
[46] T. Shido, M. Lok, R. Prins, Top. Catal. 8 (1999) 223.
[47] S. Calvin, S.X. Luo, C. Caragianis-Broadbridge, J.K. McGuinness, E. Anderson, A. Lehman, K.H. Wee, S.A. Morrison, L.K. Kurihara, Appl. Phys. Lett. 87 (2005) 1.
[48] K.S.W. Sing, D.H. Everett, R.A.W. Haul, L. Moscou, R.A. Pierotti, J. Rouquérol, T. Siemieniewska, Pure Appl. Chem. 57 (1985) 603.
[49] R.S. Zhou, R.L. Snyder, Acta Crystallogr. B 47 (1991) 617.
[50] G. Apai, J.F. Hamilton, J. Stohr, A. Thompson, Phys. Rev. Lett. 43 (1979) 165.
[51] Y. Duan, J. Li, Mater. Chem. Phys. 87 (2004) 452.
[52] S. Calvin, C.J. Riedel, E.E. Carpenter, S.A. Morrison, R.M. Stround, V.G. Harris, Phys. Scripta T115 (2005) 744.
[53] H.S. Roh, K.W. Jun, W.S. Dong, J.S. Chang, S.E. Park, Y.I. Joe, J. Mol. Catal. A 181 (2002) 137.
[54] H.S. Roh, K.W. Jun, S.C. Baek, S.E. Park, Bull. Korean Chem. Soc. 23 (2002) 1166.
[55] J. Ye, Z. Li, H. Duan, Y. Liu, J. Rare Earth 24 (2006) 302.
[56] R.C. Jin, Y.X. Chen, W.Z. Li, W. Cui, Y.Y. Ji, C.Y. Yu, Y. Jiang, Appl. Catal. A 201 (2000) 71.
[57] M.D. Gross, J.M. Vohs, R.J. Gorte, J. Mater. Chem. 17 (2007) 3071.
[58] H.S. Bengaard, J.K. Norskov, J. Sehested, B.S. Clausen, L.P. Nielsen, A.M. Molenbroek, J.R. Rostrup-Nielsen, J. Catal. 209 (2002) 365.
[59] Z.W. Liu, K.W. Jun, H.S. Roh, S.C. Baek, S.E. Park, J. Mol. Catal. A 189 (2002) 283.
[60] Y. Lu, J. Xue, C. Yu, Y. Liu, S. Shen, Appl. Catal. A 174 (1998) 121.
[61] H.S. Roh, K.W. Jun, W.S. Dong, S.E. Park, Y.I. Joe, Chem. Lett. (2001) 666.
[62] Q. Miao, G. Xiong, L. Xu, S. Sheng, X. Guo, Chin. J. Catal. 18 (1997) 17.
[63] H.T. Wang, Z.H. Li, S.X. Tian, React. Kinet. Catal. Lett. 83 (2004) 245.
[64] V.A. Tsipouriari, X.E. Verykios, Stud. Surf. Sci. Catal. 119 (1998) 795.
[65] K.C. Khulbe, R.S. Mann, Catal. Rev. 24 (1982) 311.
[66] J.H. Sinfelt, J.L. Carter, D.J.C. Yates, J. Catal. 24 (1972) 283.
[67] V. Ponec, Appl. Catal. A 222 (2001) 31.
[68] A. Roberti, V. Ponec, W.M.H. Sachtler, J. Catal. 28 (1973) 381.
[69] N.D. Lang, H. Ehreneich, Phys. Rev. 168 (1968) 605.
[70] J.H. Kim, D.J. Suh, T.J. Park, K.L. Kim, Appl. Catal. A 197 (2000) 191.
[71] Y.H. Chin, D.L. King, H.S. Roh, Y. Wang, S.M. Heald, J. Catal. 244 (2006) 153.